

Leptonic $g - 2$ anomaly in an extended Higgs sector with vector-like leptons

Hrishabh Bharadwaj,^{a,†} Sukanta Dutta,^{b,#} Ashok Goyal,^{a,\$}

^a*Department of Physics & Astrophysics, University of Delhi, Delhi, India.*

^b*SGTB Khalsa College, University of Delhi, Delhi, India.*

E-mail: [†] [Corresponding Author: hrishabhphysics@gmail.com](mailto:hrishabhphysics@gmail.com),
[#]Sukanta.Dutta@gmail.com, ^{\$}agoyal45@yahoo.com

ABSTRACT: We address the observed discrepancies in the anomalous magnetic dipole moments (MDM) of the muon and electron by extending the inert two Higgs Doublet Model (2HDM) with SM gauge singlet complex scalar field and singlet Vector-like Lepton (VLL) field. We obtain the allowed parameter space constrained from the Higgs decays to gauge Bosons at LHC, LEP II data and electro-weak precision measurements. The muon and electron MDM's are then explained within a common parameter space for different sets of allowed couplings and masses of the model particles.

KEYWORDS: Vector-like lepton, muon $g - 2$, electron $g - 2$, 2HDM

Contents

1	Introduction	1
2	The model	3
2.1	Positivity and minimisation Conditions	4
2.2	Scalar and Pseudo-scalar Mass eigenstates	5
2.3	Yukawa Couplings	7
3	Experimental Constraints	7
3.1	Higgs decays to Gauge Bosons	7
3.2	LEP II Data	11
3.3	Electroweak Precision Observables	12
4	Anomalous MDM of Leptons	15
5	Summary	18
A	Scalar Couplings in terms of Mass Parameters	19
B	Definition of Loop Form Factors	20
C	Veltman Passarino Loop Integrals	21
D	One loop and two loop functions for MDM	21

1 Introduction

The anomalous magnetic moment of the electron and muon has been measured to an unprecedented precision and its deviation with the theoretically calculated value in the Standard Model (SM) [1, 2] and it may as well be a portent of new physics beyond the SM. The estimated value of the anomalous MDM of muon [3]

$$a_{\mu}^{\text{FNAL}} = 116592040(54) \times 10^{-11} \quad (1.1)$$

from recent measurements by *G-2 Collaboration* validates the earlier observations from the Brookhaven National Laboratory E821 experiment [4, 5]. The combined measurements for μ^{-} and μ^{+} from both these experiments result in $a_{\mu}^{\text{expt}} = 116592061(41) \times 10^{-11}$ [3]. Comparing with the recent theoretical prediction in SM $a_{\mu}^{\text{SM}} = 116591810(43) \times 10^{-11}$ [6], a discrepancy of 4.2σ is observed and the deviation of anomalous MDM from SM prediction is given as [3]

$$\Delta a_{\mu} = (251 \pm 59) \times 10^{-11} \quad (1.2)$$

The principle uncertainty in the calculations of the SM contribution to a_μ arises from the hadronic vacuum polarisation and from light by light scattering contributions. Recently the Budapest-Marseille-Wuppertal collaboration [7] has computed the leading hadronic contribution to the muon anomalous MDM from lattice QCD and shown that there does not remain any discrepancy with the experiment. However, the HVP contribution has been estimated by the authors of references [8–10] indicating that this discrepancy far from being removed has only been shifted to the uncertainties in the e^+e^- data and the electroweak fit. In the absence of more reliable and independently confirmed non-perturbative QCD contribution, we will assume that BSM physics is indeed required to explain the discrepancy.

Another recent measurement of the fine structure constant α_{em} [11] has likewise resulted in a mild $\sim 2.4\sigma$ discrepancy in experimental and theoretical prediction of the electron anomalous magnetic moment

$$\Delta a_e = [-88 \pm 28 (\text{expt.}) \pm 23 (\alpha) \pm 2 (\text{theory})] \times 10^{-14} \quad (1.3)$$

It is important to note that anomalous MDM of the muon is opposite in sign to that of an electron and is much larger in magnitude that can be accounted for, by the electron mass scaling m_e^2/m_μ^2 .

Various attempts for simultaneous explanation of the leptonic anomalous magnetic moment anomalies have been made in the past several years [12–26]. Models with axion-like particles (ALP) [16], lepto-quarks [27, 30–32], vector-like leptons (VLL) [33–39] and super-symmetric models [28, 29, 40–42] have been employed with varying success to explain the anomaly.

The two Higgs doublet model (2HDM) has been extensively employed in the literature to explain the muon magnetic moment anomaly [43–52]. The 2HDM model is the simplest extension of the SM. With an appropriate Z_2 symmetry, Type-X lepton specific 2HDM model with non-SM Higgs coupling to leptons being enhanced by $\tan\beta$, has been used to explain $(g-2)_\mu$. The solution, in general, requires large value of $\tan\beta$ and a light pseudo-scalar boson. The model is however strongly constrained by lepton precision observables and only a limited parameter space is available [48, 50, 52–54].

The 2HDM model has been extended with the inclusion of a real or complex singlet scalars with appropriate Z_2 symmetry to expand the available parameter space required to explain the muon magnetic moment anomaly [22, 55]. Vector-like leptons have been introduced in the multi Higgs extension of the SM to relax the severe constraints discussed above. Inclusion of VLL in 2HDM enlarges the allowed parameter space consistent with the muon $g-2$ while still being within the theoretical and experimental bounds [33–38].

In the context of Lepton-portal Dark Matter models with the introduction of VLL or sleptons, an explanation of $(g-2)_\mu$ has been sought. It required simultaneous introduction of a VLL doublet and a singlet. In this model adherence to all experimental and theoretical bounds was found to be challenging [56].

A simultaneous explanation of the muon and electron $g-2$ anomaly was achieved in [17] by introducing a VLL doublet and a singlet in the SM. The Higgs sector itself was extended by adding complex scalars in the TeV mass range. Similar study was done in [57] where muon magnetic moment is obtained at the two-loop level with a sizable

negative contribution to electron $g-2$ in the presence of vector-like leptons. A simultaneous explanation of the muon and electron $g-2$ anomaly in an inert lepton specific 2HDM model has been achieved in [15]. In this model Z_2 symmetry is broken in the leptonic sector with non-universal Yukawa coupling between leptons and inert Higgs doublet. The model requires hierarchical couplings of inert Higgs doublet with leptons. Furthermore it was required that the Yukawa couplings for μ and e/τ leptons be opposite in sign and the parameter region was tightly constrained by Lepton flavor universality tests.

Therefore, it is worthwhile to explore the variants of 2HDM which can explain the anomalous MDMs of muon and electron. In section 2, we formulate the viable model by augmenting the inert 2HDM with a neutral complex scalar and a heavy vector-like charged lepton which are SM gauge singlets. We constrain the model parameters from Higgs decays, LEP data and precision measurements in section 3. We compute the MDM of leptons in Section 4 and conclude in Section 5.

2 The model

In order to simultaneously explain the muon and electron magnetic moment anomalies with common set of parameter values, we introduce a Z_2 symmetry in generic inert 2HDM which is allowed to be relaxed in the leptonic sector with universal Yukawa couplings. The lepton flavor universality (LFU) in the τ decays reported by the HFAG collaboration is then, trivially satisfied [58].

We begin the construction of the model by assigning the Z_2 parity quantum number for all the particle contents of the model.

Fields	Q_l	l_L	u_R	d_R	e_R	Φ_1	Φ_2	Φ_3	χ_L	χ_R	V^μ
$SU(3)_c$	3	1	3	3	1	1	1	1	1	1	G^μ
$SU(2)_L$	2	2	1	1	1	2	2	1	1	1	W_i^μ
$U(1)_Y$	$\frac{1}{6}$	$-\frac{1}{2}$	$\frac{2}{3}$	$-\frac{1}{3}$	-1	$\frac{1}{2}$	$\frac{1}{2}$	0	-1	-1	B^μ
Z_2	+	+	+	+	+	+	-	-	-	+	+

Under Z_2 symmetry all the SM particles are assumed to be even whereas, scalar second doublet Φ_2 and complex singlet Φ_3 are odd. The left and the right chiral vector-like leptons are assumed to transform differently, namely, $\chi_L \rightarrow -\chi_L$ and $\chi_R \rightarrow \chi_R$. The Z_2 symmetry ensures that the SM gauge bosons and fermions are forbidden to have direct interaction with the second (inert) Higgs doublet and additional complex scalar singlet. We however, allow soft breaking of Z_2 symmetry by the vector-like lepton mass term and an explicit breaking of Z_2 symmetry in the Yukawa Lagrangian \mathcal{L}_Y in order to facilitate coupling of SM leptons with CP odd pseudo-scalars.

The Lagrangian is written as

$$\mathcal{L} = \mathcal{L}_{\text{scalar}} + \mathcal{L}_Y + \mathcal{L}_{\text{VL}} \quad (2.1a)$$

$$\mathcal{L}_{\text{scalar}} = (D_\mu \Phi_1)^\dagger (D^\mu \Phi_1) + (D_\mu \Phi_2)^\dagger (D^\mu \Phi_2) + (D_\mu \Phi_3)^* (D^\mu \Phi_3) - V_{\text{scalar}} \quad (2.1b)$$

$$V_{\text{scalar}} = V_{2\text{HDM}}(\Phi_1, \Phi_2) + V_{\text{Singlet}}(\Phi_3) + V_{\text{Mix}}(\Phi_1, \Phi_2, \Phi_3) \quad (2.1c)$$

$$\begin{aligned} &= -\frac{1}{2}m_{11}^2 (\Phi_1^\dagger \Phi_1) - \frac{1}{2}m_{22}^2 (\Phi_2^\dagger \Phi_2) + \frac{\lambda_1}{2} (\Phi_1^\dagger \Phi_1)^2 + \frac{\lambda_2}{2} (\Phi_2^\dagger \Phi_2)^2 \\ &+ \lambda_3 (\Phi_1^\dagger \Phi_1) (\Phi_2^\dagger \Phi_2) + \lambda_4 (\Phi_1^\dagger \Phi_2) (\Phi_2^\dagger \Phi_1) + \frac{1}{2} \left[\lambda_5 (\Phi_1^\dagger \Phi_2)^2 + h.c. \right] \\ &- \frac{1}{2}m_{33}^2 \Phi_3^* \Phi_3 + \frac{\lambda_8}{2} (\Phi_3^* \Phi_3)^2 + \lambda_{11} |\Phi_1|^2 \Phi_3^* \Phi_3 + \lambda_{13} |\Phi_2|^2 \Phi_3^* \Phi_3 \\ &- i \kappa \left[(\Phi_1^\dagger \Phi_2 + \Phi_2^\dagger \Phi_1) (\Phi_3 - \Phi_3^*) \right] \end{aligned} \quad (2.1d)$$

where

$$\Phi_1 \equiv \left[\begin{array}{c} \phi_1^+ \\ \frac{1}{\sqrt{2}} (v_{\text{SM}} + \phi_1^0 + i \eta_1^0) \end{array} \right]; \quad \Phi_2 \equiv \left[\begin{array}{c} \phi_2^+ \\ \frac{1}{\sqrt{2}} (\phi_2^0 + i \eta_2^0) \end{array} \right] \quad \text{and} \quad \Phi_3 \equiv \frac{1}{\sqrt{2}} [v_s + \phi_3^0 + i \eta_3^0] \quad (2.1e)$$

$$-\mathcal{L}_Y = y_u \overline{Q}_L \widetilde{\Phi}_1 u_R + y_d \overline{Q}_L \Phi_1 d_R + y_l \overline{L} \Phi_1 e_R + y_1 \overline{L} \Phi_2 e_R + h.c. \quad (2.1f)$$

$$\mathcal{L}_{\text{VL}} = \bar{\chi} i \left(\not{\partial} - ig' \frac{Y}{2} \mathcal{B} \right) \chi - m_\chi \bar{\chi} \chi - y_2 \overline{\chi}_L \chi_R \Phi_3 - y_3 \overline{\chi}_L e_R \Phi_3 \quad (2.1g)$$

where all couplings in the scalar potential and Yukawa sector are real in order to preserve the CP invariance. The quartic scalar couplings are taken to be perturbative i.e. $|\lambda_i| \leq 4\pi$. Here, we have invoked an additional global $U(1)$ symmetry such that $\Phi_3 \rightarrow e^{i\alpha} \Phi_3$ to reduce the number of free parameters in the scalar potential, which is however allowed to be softly broken by the κ term and Yukawa couplings y_2 and y_3 .

2.1 Positivity and minimisation Conditions

In order to have a stable minimum (*i.e.* potential bounded from below), the parameters of the potential need to satisfy positivity conditions which are essentially governed by the quartic terms in the scalar potential. The co-positivity conditions for the Lagrangian given in (2.1d) are obtained by demanding the determinant and principal minors of the Hessian to be positive definite. The couplings are then required to satisfy

$$\mathcal{H} = \begin{vmatrix} \lambda_1 & \lambda_3 + \lambda_4 - |\lambda_5| & \lambda_{11} \\ \lambda_3 + \lambda_4 - |\lambda_5| & \lambda_2 & \lambda_{13} \\ \lambda_{11} & \lambda_{13} & \lambda_8 \end{vmatrix} > 0 \quad (2.2)$$

along with λ_1, λ_2 and $\lambda_8 > 0$. This leads to the following co-positivity conditions:

$$\lambda_1, \lambda_2, \lambda_8 > 0, \quad (2.3a)$$

$$\bar{\lambda}_{12} \equiv \lambda_3 + \Theta[|\lambda_5| - \lambda_4] (\lambda_4 - |\lambda_5|) + \sqrt{\lambda_1 \lambda_2} > 0, \quad (2.3b)$$

$$\bar{\lambda}_{13} \equiv \lambda_{11} + \sqrt{\lambda_1 \lambda_8} > 0, \quad (2.3c)$$

$$\bar{\lambda}_{23} \equiv \lambda_{13} + \sqrt{\lambda_2 \lambda_8} > 0 \text{ and} \quad (2.3d)$$

$$\sqrt{\lambda_1 \lambda_2 \lambda_8} + [\lambda_3 + \Theta[|\lambda_5| - \lambda_4](\lambda_4 - |\lambda_5|)]\sqrt{\lambda_8} + \lambda_{11}\sqrt{\lambda_2} + \sqrt{2\bar{\lambda}_{12}\bar{\lambda}_{13}\bar{\lambda}_{23}} > 0 \quad (2.3e)$$

Considering the VEV's for Φ_1 and Φ_3 to be real, we minimise the scalar potential (2.1d) which leads to the following two minimisation conditions:

$$m_{11}^2 = \lambda_1 v_{\text{SM}}^2 + \lambda_{11} v_s^2 \quad (2.4a)$$

$$m_{33}^2 = \lambda_8 v_s^2 + \lambda_{11} v_{\text{SM}}^2 \quad (2.4b)$$

The m_{22}^2 parameter remains unconstrained by the extremum condition.

2.2 Scalar and Pseudo-scalar Mass eigenstates

The squared-mass matrix constructed from all six scalar components of the scalar fields is given by

$$M_{\phi_i \phi_j}^2 = \left. \frac{\partial^2 V}{\partial \phi_i \partial \phi_j} \right|_{\Phi_i = \langle \Phi_i \rangle}, \quad \text{for } i, j \equiv 1, \dots, 6 \quad (2.5)$$

with ϕ_i being the respective scalar and/ or pseudo-scalar fields as defined in equation (2.1e).

As there is no mixing among the imaginary component of the inert doublet with the real component of either the first SM like doublet or the singlet, the two mass matrices for neutral scalars and pseudo-scalars are therefore completely decoupled.

The 2×2 CP-even neutral scalar mass matrix arises due to the mixing of the real components of SM like first doublet Φ_1 and the singlet Φ_3 and is given as

$$M_{\phi_1^0 \phi_3^0}^2 = \frac{1}{2} \begin{pmatrix} \phi_1^0 & \phi_3^0 \end{pmatrix} \begin{pmatrix} \lambda_1 v_{\text{SM}}^2 & \lambda_{11} v_{\text{SM}} v_s \\ \lambda_{11} v_{\text{SM}} v_s & \lambda_8 v_s^2 \end{pmatrix} \begin{pmatrix} \phi_1^0 \\ \phi_3^0 \end{pmatrix} \quad (2.6)$$

On diagonalising the CP-even mass matrix by orthogonal rotation matrix parameterised in terms of the mixing angle θ_{13} we get the two mass eigenstates h_1 and h_3 . The mass eigenvalues are

$$m_{h_1}^2 = \cos^2 \theta_{13} \lambda_1 v_{\text{SM}}^2 + \sin(2\theta_{13}) v_s \lambda_{11} v_{\text{SM}} + \sin^2 \theta_{13} v_s^2 \lambda_8 \quad (2.7a)$$

$$m_{h_3}^2 = \sin^2 \theta_{13} \lambda_1 v_{\text{SM}}^2 - \sin(2\theta_{13}) v_s \lambda_{11} v_{\text{SM}} + \cos^2 \theta_{13} v_s^2 \lambda_8 \quad (2.7b)$$

The vanishing off diagonal term of the diagonalised mass matrix defines the mixing angle in terms of other model parameters as follows:

$$\tan 2\theta_{13} = \frac{\lambda_{11} v_{\text{SM}} v_s}{\lambda_1 v_{\text{SM}}^2 - \lambda_8 v_s^2} \quad (2.7c)$$

Similarly, we diagonalise the following mass matrix for CP-odd scalars η_2^0 and η_3^0 by the orthogonal rotation matrix parameterised by mixing angle θ_{23}

$$\frac{1}{2} \begin{pmatrix} \eta_2^0 & \eta_3^0 \end{pmatrix} \begin{pmatrix} -\frac{1}{2}m_{22}^2 + \frac{1}{2}\bar{\lambda}_{345}v_{\text{SM}}^2 + \frac{1}{2}v_s^2\lambda_{13} & -\sqrt{2}\kappa v_{\text{SM}} \\ -\sqrt{2}\kappa v_{\text{SM}} & 0 \end{pmatrix} \begin{pmatrix} \eta_2^0 \\ \eta_3^0 \end{pmatrix} \quad (2.8)$$

where $\bar{\lambda}_{345} = \lambda_3 + \lambda_4 - \lambda_5$. The mass eigenvalues of the pseudo-scalar mass eigenstates A^0 and P^0 are calculated to be

$$m_{A^0}^2 = \frac{1}{2} (\bar{\lambda}_{345}v_{\text{SM}}^2 - m_{22}^2 + \lambda_{13}v_s^2) \cos^2 \theta_{23} - \sqrt{2}\kappa v_{\text{SM}} \sin 2\theta_{23} \quad (2.9a)$$

$$m_{P^0}^2 = \frac{1}{2} (\bar{\lambda}_{345}v_{\text{SM}}^2 - m_{22}^2 + \lambda_{13}v_s^2) \sin^2 \theta_{23} + \sqrt{2}\kappa v_{\text{SM}} \sin 2\theta_{23} \quad (2.9b)$$

The off-diagonal vanishing terms relates the mixing angle θ_{23} to the other mass and model parameters as:

$$\kappa = -\frac{1}{2\sqrt{2}v_{\text{SM}}} (m_{P^0}^2 + m_{A^0}^2) \tan(2\theta_{23}) \quad (2.9c)$$

Defining the remaining neutral and charged saclar mass eigenstates as

$$\begin{aligned} \phi_2^0 &\rightarrow h_2 \\ \eta_1^0 &\rightarrow G^0 \text{ (massless Nambu-Goldstone Boson)} \\ \phi_1^\pm &\rightarrow G^\pm \text{ (massless Nambu-Goldstone Boson)} \\ \phi_2^\pm &\rightarrow H^\pm \end{aligned}$$

with

$$m_{h_2}^2 = \frac{1}{2} [-m_{22}^2 + (\lambda_3 + \lambda_4 + \lambda_5) v_{\text{SM}}^2 + \lambda_{13}v_s^2] \quad (2.10a)$$

$$m_{H^\pm}^2 = -m_{22}^2 + \lambda_3 v_{\text{SM}}^2 + \lambda_{13}v_s^2 \quad (2.10b)$$

The twelve independent parameters in the scalar potential (2.1d),

$$m_{11}, m_{22}, m_{33}, \lambda_{i=1,\dots,5}, \lambda_8, \lambda_{11}, \lambda_{13} \text{ and } \kappa \quad (2.11)$$

can now be expressed in terms of the following physical masses and mixing angles:

$$v_{\text{SM}}, v_s, m_{h_1}^2, m_{h_2}^2, m_{H^\pm}^2, m_{A^0}^2, m_{P^0}^2, \theta_{13}, \theta_{23} \text{ and } m_{22}^2 \quad (2.12)$$

These mass relations are given in the Appendix A.

Substituting the mass relations of λ_4 and λ_5 from equations (A.5) and (A.6) respectively in the theta function appearing in equation (2.3b) of the co-positivity conditions. we get two mutually exclusive allowed regions of parameter space:

$$\Theta(|\lambda_5| - \lambda_4) = \begin{cases} \Theta [m_{H^\pm}^2 - (m_{A^0}^2 + m_{P^0}^2)] & \text{for } m_{h_2}^2 > m_{A^0}^2 + m_{P^0}^2 \\ \Theta [m_{h_2}^2 - m_{H^\pm}^2] & \text{for } m_{h_2}^2 < m_{A^0}^2 + m_{P^0}^2 \end{cases} \quad (2.13)$$

In this article we explore the phenomenologically interesting region where $m_{H^\pm}^2 > m_{A^0}^2 + m_{P^0}^2$.

2.3 Yukawa Couplings

The Yukawa interactions given in (2.1f) and (2.1g) can be re-written as

$$-\mathcal{L}_{\text{SM Fermions}}^{\text{Yukawa}} = \sum_{s_i \equiv h_1, h_3} \frac{y_{ffs_i}}{\sqrt{2}} (v_{\text{SM}} \delta_{s_i, h_1} + s_i) \bar{f} f + \frac{y_{llh_2}}{\sqrt{2}} h_2 \bar{l}^- l^- \sum_{s_i \equiv P^0, A^0} \frac{y_{lls_i}}{\sqrt{2}} s_i \bar{l}^- \gamma_5 l^- + [y_{l\nu H^-} \bar{\nu}_l P_R l^- H^+ + \text{h.c.}] \quad (2.14a)$$

$$-\mathcal{L}_{\text{VL Leptons}}^{\text{Yukawa}} = \sum_{s_i \equiv h_1, h_3, A^0, P^0} \frac{1}{\sqrt{2}} (v_s \delta_{s_i, h_3} + s_i) \bar{\chi} (y_{\chi\chi s_i} P_R + y_{\chi\chi s_i}^* P_L) \chi \quad (2.14b)$$

$$-\mathcal{L}_{\text{VL, SM Leptons}}^{\text{Yukawa}} = \sum_{s_i \equiv h_1, h_3, A^0, P^0} \frac{1}{\sqrt{2}} (v_s \delta_{s_i, h_3} + s_i) [y_{l\chi s_i} \bar{\chi} P_R l^- + \text{h.c.}] \quad (2.14c)$$

where f and l^- represent SM fermions and SM charged leptons respectively. The Yukawa couplings $y_{\psi_1 \psi_2 S_i}$ with scalar/ pseudoscalar mass eigenstates are given in Table 1.

y_{ffh_1}	$(\sqrt{2}m_f/v_{\text{SM}}) \cos \theta_{13}$	y_{llh_2}	y_1
y_{ffh_3}	$-(\sqrt{2}m_f/v_{\text{SM}}) \sin \theta_{13}$	y_{llP^0}	$-i y_1 \sin \theta_{23}$
$y_{\chi\chi h_1}$	$y_2 \sin \theta_{13}$	y_{llA^0}	$i y_1 \cos \theta_{23}$
$y_{\chi\chi h_3}$	$y_2 \cos \theta_{13}$	$y_{l\chi h_1}$	$y_3 \sin \theta_{13}$
$y_{\chi\chi P^0}$	$i y_2 \cos \theta_{23}$	$y_{l\chi h_3}$	$y_3 \cos \theta_{13}$
$y_{\chi\chi A^0}$	$i y_2 \sin \theta_{23}$	$y_{l\chi P^0}$	$i y_3 \cos \theta_{23}$
$y_{l\nu H^-}$	y_1	$y_{l\chi A^0}$	$i y_3 \sin \theta_{23}$

Table 1: Yukawa couplings

3 Experimental Constraints

Any model beyond the SM has to satisfy the existing theoretical and experimental observations. In this section, we subject the model discussed in section 2 to the observations of SM-like Higgs mass and signal strengths as measured at the LHC Run-II and at the ILC. We further examine the electroweak precision constraints on the masses of scalars and pseudo-scalars from the direct production at LEP-II.

3.1 Higgs decays to Gauge Bosons

Any multi-Higgs model has to accommodate the SM like Higgs with the mass and signal strengths measured at the LHC [59] with the future prospects of increasing precision measurements at the future collider experiments. We identify and align the CP even lightest scalar mass eigenstate h_1 with 125.09 GeV SM Higgs. Therefore, the couplings of the h_1 with a pair of fermions and gauge bosons are essentially those of SM Higgs couplings but suppressed by $\cos \theta_{13}$ due to $\Phi_1 - \Phi_3$ small angle mixing ($\theta_{13} = 0$ restores the full SM Higgs).

We compare the total Higgs decay width in SM $\Gamma(h^{\text{SM}} \rightarrow \text{all}) \sim 4.07$ MeV [60, 61] with the recently measured total decay width $\Gamma(h_1 \rightarrow \text{all}) \sim 3.2_{-2.2}^{+2.8}$ MeV at the LHC [59].

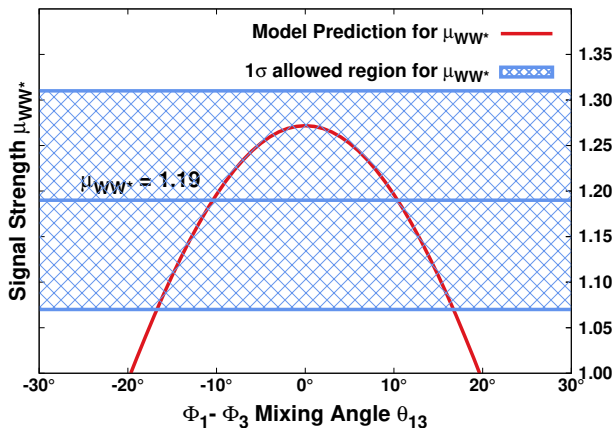


Figure 1: Variation of μ_{WW^*} with the CP-even mixing angle θ_{13} is shown with the dashed red line. The allowed shaded one sigma region for measured $\mu_{WW^*} = 1.19 \pm 0.12$ [59] is also shown.

Assuming, that the model can account for the measured value of the total decay width, we constrain the model parameters by examining the bounds on the partial decay widths of decay channels for 125 GeV h_1 at LHC. To this end, we define the signal strength μ_{XY} *w.r.t.* h_1 production *via* dominant gluon fusion in $p - p$ collision, followed by its decay to X & Y pairs in the narrow width approximation as

$$\begin{aligned} \mu_{XY} &= \frac{\sigma(pp \rightarrow h_1 \rightarrow XY)}{\sigma(pp \rightarrow h \rightarrow XY)^{\text{SM}}} = \frac{\Gamma(h_1 \rightarrow gg)}{\Gamma(h^{\text{SM}} \rightarrow gg)} \frac{\text{BR}(h_1 \rightarrow XY)}{\text{BR}(h^{\text{SM}} \rightarrow XY)} \\ &= \cos^4 \theta_{13} \frac{\Gamma(h^{\text{SM}} \rightarrow \text{all})}{\Gamma(h_1 \rightarrow \text{all})} \end{aligned} \quad (3.1)$$

We first analyse the partial decay width of $h_1 \rightarrow WW^*$ channel which solely depends on θ_{13} :

$$\Gamma(h_1 \rightarrow WW^*) = \cos^2 \theta_{13} \Gamma(h^{\text{SM}} \rightarrow WW^*) \quad (3.2)$$

Among the signal strengths for Higgs decaying to gauge Bosons at tree level, $\mu_{WW^*} \sim 1.19 \pm 0.12$ [59] has the least uncertainty for which it can provide the strongest upper bound on the mixing angle θ_{13} . In figure 1, we show the one sigma band around the central value of the μ_{WW^*} which restricts the model contribution curve drawn in green for $|\theta_{13}| \lesssim 10^\circ$ at 1σ level.

Next, we calculate the partial decay widths generated at one loop for $h_1 \rightarrow \gamma\gamma$ and $h_1 \rightarrow Z\gamma$ respectively. The contribution of charged scalars H^\pm and vector-like leptons χ^- modify the SM predictions for the branching ratios. The partial decay widths for $\gamma\gamma$ and $Z\gamma$ in the model are parameterised as

$$\Gamma(h_1 \rightarrow \gamma\gamma) = \cos^2 \theta_{13} |1 + \zeta_{\gamma\gamma}|^2 \Gamma(h^{\text{SM}} \rightarrow \gamma\gamma) \quad (3.3a)$$

$$\Gamma(h_1 \rightarrow Z\gamma) = \cos^2 \theta_{13} |1 + \zeta_{Z\gamma}|^2 \Gamma(h^{\text{SM}} \rightarrow Z\gamma) \quad (3.3b)$$

where the SM Higgs partial decay widths in $\gamma\gamma$ and $Z\gamma$ channels are given as

$$\Gamma(h^{\text{SM}} \rightarrow \gamma\gamma) = \frac{G_F \alpha^2 m_h^3}{128 \sqrt{2} \pi^3} \left| \frac{4}{3} \mathcal{M}_{1/2}^{\gamma\gamma} \left(\frac{4m_t^2}{m_h^2} \right) + \mathcal{M}_1^{\gamma\gamma} \left(\frac{4m_W^2}{m_h^2} \right) \right|^2 \quad (3.4a)$$

$$\Gamma(h^{\text{SM}} \rightarrow Z\gamma) = \frac{G_F^2 \alpha m_W^2 m_h^3}{64 \pi^4} \left(1 - \frac{m_Z^2}{m_h^2} \right)^3 \left| 2 \frac{(1 - \frac{8}{3} s_W^2)}{c_W} \mathcal{M}_{1/2}^{Z\gamma} \left(\frac{4m_t^2}{m_h^2}, \frac{4m_t^2}{m_Z^2} \right) + \mathcal{M}_1^{Z\gamma} \left(\frac{4m_W^2}{m_h^2}, \frac{4m_W^2}{m_Z^2} \right) \right|^2 \quad (3.4b)$$

The dimensionless parameters $\zeta_{\gamma\gamma}$ and $\zeta_{Z\gamma}$ are defined as

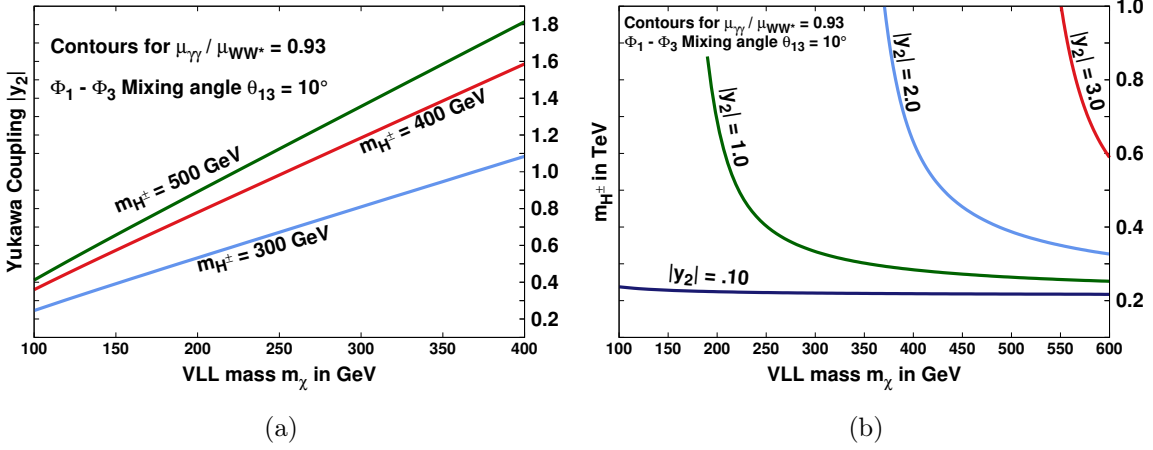


Figure 2: Contours satisfying the constraint $\mu_{\gamma\gamma}/\mu_{WW^*} = 0.93^{+0.17}_{-0.16}$ [59] for $\theta_{13} = 10^\circ$ are drawn in (a) $m_\chi - |y_2|$ plane corresponding to three choices of charged Higgs mass and (b) $m_\chi - m_{H^\pm}$ plane corresponding to four choices of $|y_2|$.

$$\zeta_{\gamma\gamma} = \frac{v_{\text{SM}}}{\cos \theta_{13}} \left[\frac{\frac{g_{h_1 H^+ H^-}}{2 m_{H^\pm}^2} \mathcal{M}_0^{\gamma\gamma} \left(\frac{4m_{H^\pm}^2}{m_{h_1}^2} \right) + \frac{y_2}{\sqrt{2} m_\chi} \sin \theta_{13} \mathcal{M}_{1/2}^{\gamma\gamma} \left(\frac{4m_\chi^2}{m_{h_1}^2} \right)}{\mathcal{M}_1^{\gamma\gamma} \left(\frac{4m_W^2}{m_{h_1}^2} \right) + \frac{4}{3} \mathcal{M}_{1/2}^{\gamma\gamma} \left(\frac{4m_t^2}{m_{h_1}^2} \right)} \right] \quad (3.5a)$$

$$\zeta_{Z\gamma} = \frac{v_{\text{SM}}}{\cos \theta_{13}} \left[\frac{-\frac{g_{h_1 H^+ H^-}}{2 m_{H^\pm}^2} \frac{1-2s_W^2}{c_W} \mathcal{M}_0^{Z\gamma} \left(\frac{4m_{H^\pm}^2}{m_{h_1}^2}, \frac{4m_{H^\pm}^2}{m_Z^2} \right) - \frac{y_2}{\sqrt{2} m_\chi} \sin \theta_{13} \frac{4 s_W^2}{c_W} \mathcal{M}_{1/2}^{Z\gamma} \left(\frac{4m_\chi^2}{m_{h_1}^2}, \frac{4m_\chi^2}{m_Z^2} \right)}{2 \frac{(1 - \frac{8}{3} s_W^2)}{c_W} \mathcal{M}_{1/2}^{Z\gamma} \left(\frac{4m_t^2}{m_{h_1}^2}, \frac{4m_t^2}{m_Z^2} \right) + \mathcal{M}_1^{Z\gamma} \left(\frac{4m_W^2}{m_{h_1}^2}, \frac{4m_W^2}{m_Z^2} \right)} \right] \quad (3.5b)$$

where the triple scalar coupling $g_{h_1 H^+ H^-} = (v_{\text{SM}} \lambda_3 \cos \theta_{13} + v_s \lambda_{13} \sin \theta_{13})$. The form factors $\mathcal{M}_{0,1/2,1}^{\gamma\gamma}$ and $\mathcal{M}_{0,1/2,1}^{Z\gamma}$ are defined in the appendix B. The analytical expressions for the partial widths except the additional contribution from VLL are identical to that given in the reference [62].

Using the analytical expressions for the partial decay widths for $h_1 \rightarrow \gamma\gamma$, $h_1 \rightarrow Z\gamma$ and $h_1 \rightarrow WW^*$ in equations (3.3a), (3.3b) and (3.2) respectively, we consider the two

ratios of the signal strengths namely,

$$\frac{\mu_{\gamma\gamma}}{\mu_{WW^*}} = \frac{\Gamma(h_1 \rightarrow \gamma\gamma)}{\Gamma(h_1 \rightarrow WW^*)} \times \frac{\Gamma(h^{\text{SM}} \rightarrow WW^*)}{\Gamma(h^{\text{SM}} \rightarrow \gamma\gamma)} = |1 + \zeta_{\gamma\gamma}|^2 \quad (3.6a)$$

$$\frac{\mu_{Z\gamma}}{\mu_{WW^*}} = \frac{\Gamma(h_1 \rightarrow Z\gamma)}{\Gamma(h_1 \rightarrow WW^*)} \times \frac{\Gamma(h^{\text{SM}} \rightarrow WW^*)}{\Gamma(h^{\text{SM}} \rightarrow Z\gamma)} = |1 + \zeta_{Z\gamma}|^2 \quad (3.6b)$$

The experimental limits on $\mu_{\gamma\gamma} = 1.11^{+0.10}_{-0.09}$ and $\mu_{WW^*} = 1.19 \pm 0.12$ for $m_{h^{\text{SM}}} = 125.09$ GeV [59] are then substituted in equations (3.6a) to constrain the allowed parameter space for the Charged Higgs and singlet vector like lepton respectively. Since experimental uncertainty for $\mu_{Z\gamma} < 6.6$ [59] is large, we do not constrain the model parameters from $h_1 \rightarrow Z\gamma$ decay channel.

We depict the contours satisfying $\mu_{\gamma\gamma}/\mu_{WW^*} = 0.93^{+0.17}_{-0.16}$ for $\theta_{13} = 10^\circ$ in figure 2. In figure 2a contours satisfying the central value of the ratio are drawn in the $m_\chi - |y_2|$ plane for $m_{H^\pm} = 300, 400$ and 500 GeV. The sensitivity of the charged Higgs mass are studied *w.r.t.* variation of the VLL mass from the contours satisfying the central value of the ratio in figure 2b for four choices of Yukawa couplings $|y_2|$ varying between 0.1 and the perturbative limit $\sqrt{4\pi}$.

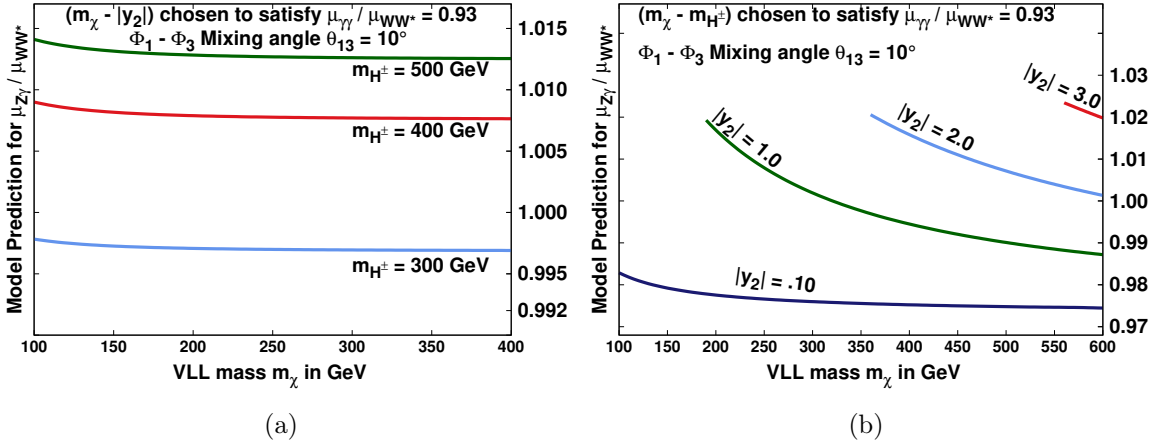


Figure 3: Variation of the ratio $\mu_{Z\gamma}/\mu_{WW^*}$ with varying m_χ for $\theta_{13} = 10^\circ$. The values of $(m_\chi, |y_2|)$ in figure (a) and that of (m_χ, m_{H^\pm}) in figure (b) are such that they satisfy the constraint $\mu_{\gamma\gamma}/\mu_{WW^*} = 0.93^{+0.17}_{-0.16}$ [59] as depicted in figures 2a and 2b respectively.

With the constrained parameter space from $\mu_{\gamma\gamma}$ and μ_{WW^*} , we estimate the ratio of signal strengths $\mu_{Z\gamma}/\mu_{WW^*}$ and make a prediction for the future improved measurements with higher luminosity and kinematic reach at FCC-hh. In figure 3 we study the variation of the ratio $\mu_{Z\gamma}/\mu_{WW^*}$ with varying m_χ for fixed $\theta_{13} = 10^\circ$. The curves in figure 3a are depicted using those $(m_\chi, |y_2|)$ values which satisfy the constraint $\mu_{\gamma\gamma}/\mu_{WW^*} = 0.93^{+0.17}_{-0.16}$ as shown in the figure 2a corresponding to $m_{H^\pm} = 300, 400$ and 500 GeV respectively. Similarly, the graphs in figure 3b are depicted using those (m_χ, m_{H^\pm}) values which satisfy the constraint $\mu_{\gamma\gamma}/\mu_{WW^*} = 0.93^{+0.17}_{-0.16}$ as shown in the figure 2b corresponding to $|y_2| = 0.1, 1.0, 2.0$ and 3.0 respectively.

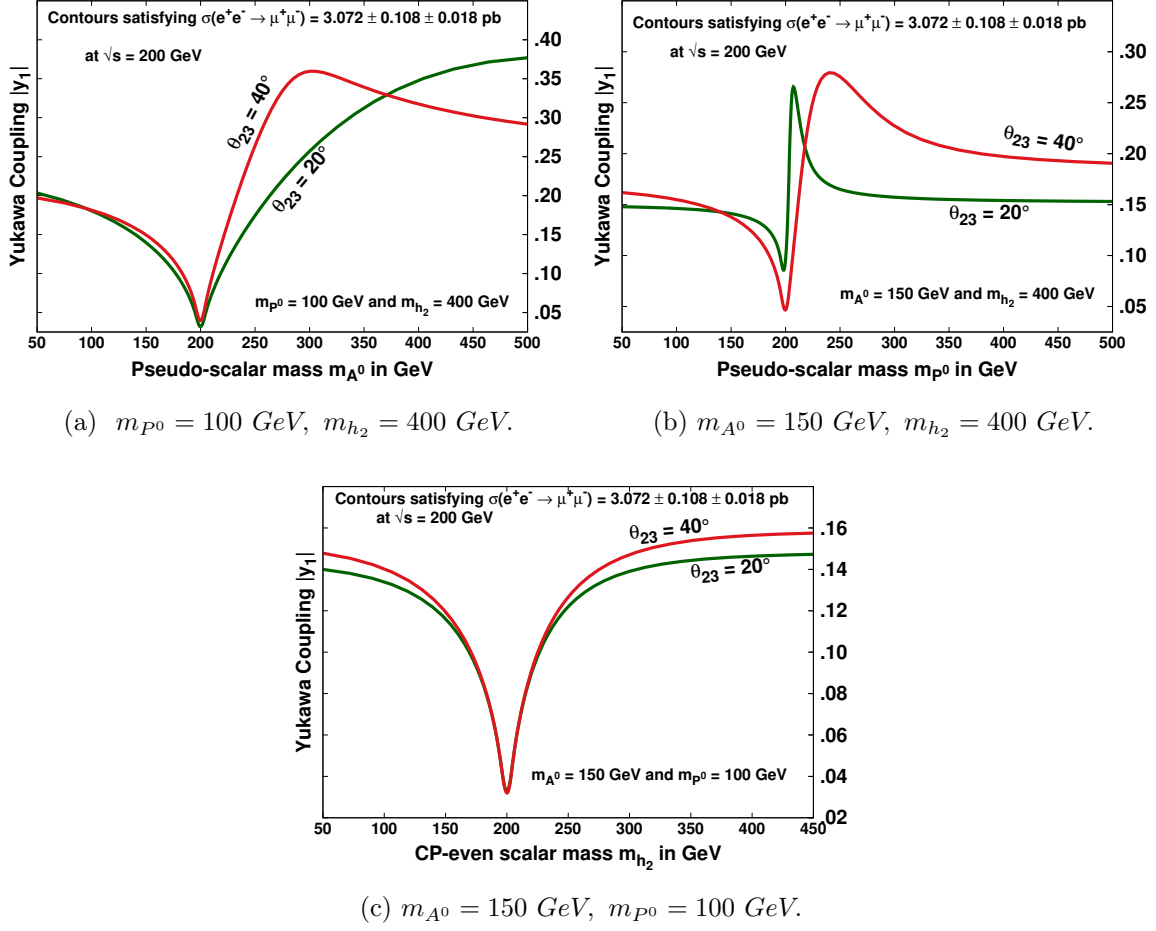


Figure 4: Contours in the plane defined by scalar/ pseudo-scalar mass and its coupling $|y_1|$ with SM leptons satisfying the combined analysis of DELPHI and L3 $\sigma(e^+ e^- \rightarrow \mu^+ \mu^-) = 3.072 \pm 0.108 \pm 0.018 \text{ pb}$ at $\sqrt{s} = 200 \text{ GeV}$ [63] for three benchmark points corresponding to two choices of the mixing angle $\theta_{23} = 20^\circ$ and 40° respectively. The parameter space lying above the contour are forbidden by LEP observations.

3.2 LEP II Data

We validate the model from the existing LEP II data and put the lower mass bounds on the scalar and pseudo-scalar mass eigenstates. This can be achieved either by investigating the (a) direct pair production of scalars and pseudo-scalars or (b) by production of pair of fermions mediated by these additional exotic physical scalars or pseudo-scalars. VLL below 100 GeV cannot be constrained by LEP experiment as they do not couple to SM particles except h_1 (SM Like Higgs) at tree level and therefore the cross-section is expected to be highly suppressed due to the electron Yukawa coupling.

The dominant direct pair production channels at e^+e^- collider:

$$e^+ e^- \rightarrow \gamma^*/Z^* \rightarrow H^+ + H^- \quad (3.7)$$

$$\text{and } e^+ e^- \rightarrow Z^* \rightarrow A^0/P^0 + h_i \quad (3.8)$$

have been studied to put the lower mass bounds on $m_{H^\pm} \gtrsim 93.5$ GeV and $\sum m_{h_i} \gtrsim 200$ GeV [63].

We compute the cross-section for $e^+ e^- \rightarrow \mu^+ \mu^-$ from the combined analysis at LEP II which is found to be $\sigma(e^+ e^- \rightarrow \mu^+ \mu^-) = 3.072 \pm 0.108 \pm 0.018$ pb at $\sqrt{s} = 200$ GeV.

The additional contribution to μ -pair production cross-section in our model can be written as:

$$\sigma_{\mu^+\mu^-}^{\text{NP}} \simeq \frac{s}{64\pi} \sqrt{\frac{1 - 4\frac{m_\mu^2}{s}}{1 - 4\frac{m_e^2}{s}}} y_1^4 \left[\left\{ \frac{\cos^2 \theta_{23}}{s - m_{A^0}^2} + \frac{\sin^2 \theta_{23}}{s - m_{P^0}^2} \right\}^2 + \frac{1}{(s - m_{h_2}^2)^2} \right] \quad (3.9)$$

where we have dropped the interference terms of h_2 with h_1 and h_3 as they are suppressed by $(m_e m_\mu)/v_{\text{SM}}^2$. Also, the contributions from h_1 and h_3 and their interference are suppressed by factor of $(m_e m_\mu)^2/v_{\text{SM}}^4$ and hence have not been taken into account. The other interference terms with γ^*/Z vanish. The interference term among scalars and pseudo-scalars vanish.

We compare the measured cross-section from the combined analysis of DELPHI and L3 at LEP II $\sigma(e^+ e^- \rightarrow \mu^+ \mu^-) = 3.072 \pm 0.108 \pm 0.018$ pb at $\sqrt{s} = 200$ GeV [63] with the model contribution as calculated in equation (3.9) for three benchmark points of the parameter space. For each such bench mark point we plot two contours corresponding to the mixing angle $\theta_{23} = 10^\circ$ and 40° respectively in (a) $m_{A^0} - |y_1|$ plane, (b) $m_{P^0} - |y_1|$ plane and (c) $m_{h_2} - |y_1|$ plane in figures 4a, 4b and 4c respectively. The parameter space below the respective contour is allowed from LEP measurements.

3.3 Electroweak Precision Observables

In this subsection we compute the additional contribution to the precision observables from heavy physical mass eigenstates $m_{h_i, P^0, A^0, \chi} \gg m_Z$. We constrain the scalar/ pseudo-scalar masses and their mixing angles based on the available electroweak precision data. Contributions to the oblique radiative corrections are given in terms of three precision parameters known as S , T and U [64–68].

The precision observables derived from the radiative corrections of the gauge Boson propagator are essentially the two point vacuum polarization tensor functions of $\Pi_{ij}^{\mu\nu}(q^2)$ where q is the four-momentum of the vector boson ($V = W, Z$ or γ). Following the prescription of the reference [69] the vacuum polarization tensor functions corresponding to pair of gauge Bosons $V_i - V_j$ can be written as

$$i\Pi_{ij}^{\mu\nu}(q) = ig^{\mu\nu} A_{ij}(q^2) + iq^\mu q^\nu B_{ij}(q^2) \quad \text{where} \quad (3.10a)$$

$$A_{ij}(q^2) = A_{ij}(0) + q^2 F_{ij}(q^2) \quad (3.10b)$$

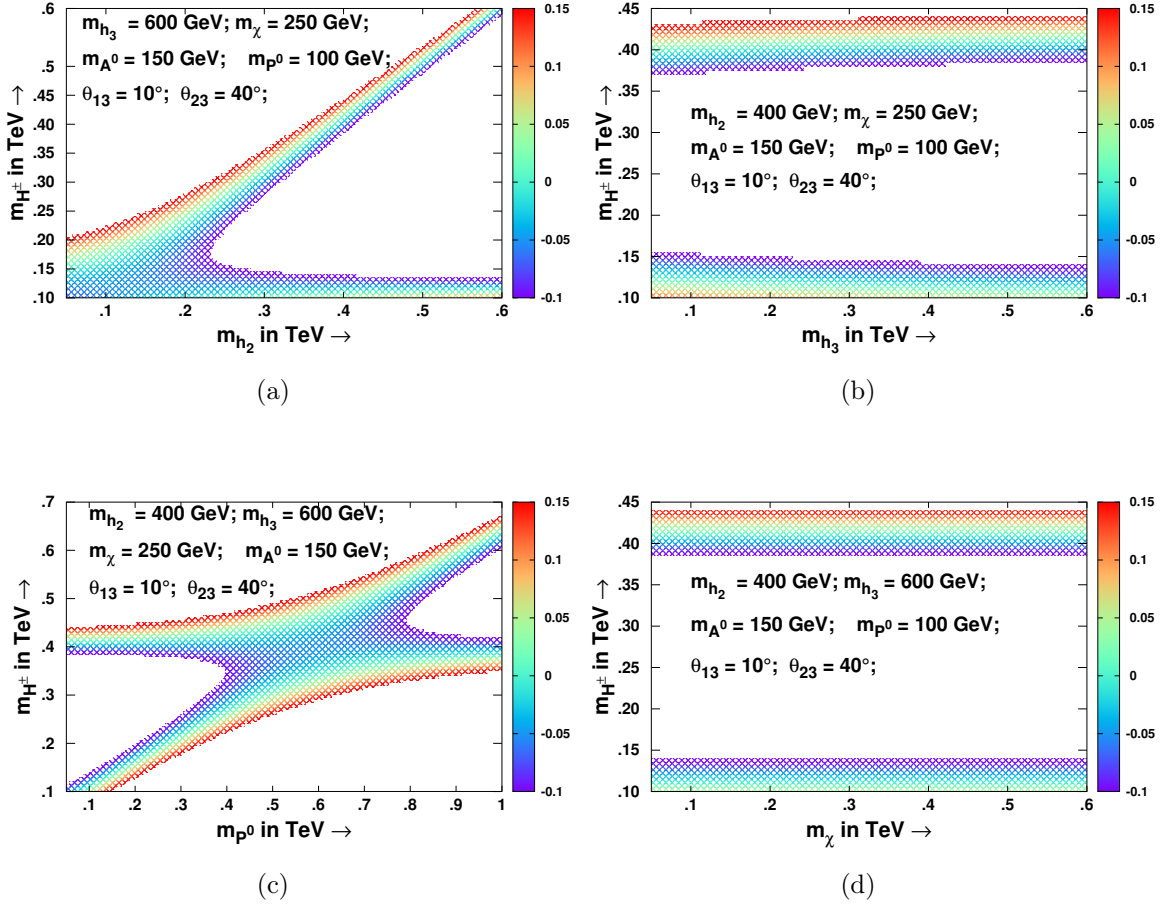


Figure 5: One sigma shaded density maps in the plane defined by respective scalar/ pseudo-scalar/ VLL masses and charged Higgs mass m_{H^\pm} satisfying the present experimental constraint on precision variable $\Delta T = 0.03 \pm 0.12$ [59].

where only $A_{ij}(q^2)$ are the relevant functions for the computation of precision observables. The equation (3.10b) defines the function F_{ij} . Accordingly the precision parameters are defined as:

$$S \equiv \frac{1}{g^2} (16\pi \cos^2 \theta_W) \left[F_{ZZ}(m_Z^2) - F_{\gamma\gamma}(m_Z^2) + \left(\frac{2 \sin^2 \theta_W - 1}{\sin \theta_W \cos \theta_W} \right) F_{Z\gamma}(m_Z^2) \right] \quad (3.11a)$$

$$T \equiv \frac{1}{\alpha_{em}} \left[\frac{A_{WW}(0)}{m_W^2} - \frac{A_{ZZ}(0)}{m_Z^2} \right] \quad (3.11b)$$

$$U \equiv \frac{1}{g^2} (16\pi) \left[F_{WW}(m_W^2) - F_{\gamma\gamma}(m_W^2) - \frac{\cos \theta_W}{\sin \theta_W} F_{Z\gamma}(m_W^2) \right] - S. \quad (3.11c)$$

where α_{em} is the fine structure constant. It is worthwhile to mention that although $A_{ij}(0)$ and F_{ij} are divergent by themselves but the total divergence associated with each precision parameter in equations (3.11a), (3.11b) and (3.11c) vanish on taking into account a gauge invariant set of one loop diagrams contributing for a given pair of gauge Bosons.

The deviation from the predicted SM contribution for S and T parameters can be expressed analytically in terms of standard Veltman-Passarrino integrals A_0 , B_0 and B_{22} defined in the appendix C:

$$\begin{aligned} \Delta S = & \frac{G_F \alpha_{em}^{-1}}{2\sqrt{2} \pi^2} \sin^2(2\theta_W) \left[\sin^2 \theta_{13} \left\{ m_Z^2 \left(\mathcal{B}_0(m_Z^2; m_Z^2, m_{h_1}^2) - \mathcal{B}_0(m_Z^2; m_Z^2, m_{h_3}^2) \right) \right. \right. \\ & \left. \left. + \mathcal{B}_{22}(m_Z^2; m_Z^2, m_{h_3}^2) - \mathcal{B}_{22}(m_Z^2; m_Z^2, m_{h_1}^2) \right\} \right. \\ & \left. + \sin^2 \theta_{23} \left(\mathcal{B}_{22}(m_Z^2; m_{h_2}^2, m_{P_0}^2) - \mathcal{B}_{22}(m_Z^2; m_{H^\pm}^2, m_{H^\pm}^2) \right) \right] \end{aligned} \quad (3.12a)$$

where

$$\mathcal{B}_{22}(q^2; m_1^2, m_2^2) \equiv B_{22}(q^2; m_1^2, m_2^2) - B_{22}(0; m_1^2, m_2^2) \quad (3.12b)$$

$$\mathcal{B}_0(q^2; m_1^2, m_2^2) \equiv B_0(q^2; m_1^2, m_2^2) - B_0(0; m_1^2, m_2^2) \quad (3.12c)$$

$$\begin{aligned} \Delta T = & \frac{G_F \alpha_{em}^{-1}}{2\sqrt{2} \pi^2} \left[\sin^2 \theta_{13} \left\{ m_W^2 \left(B_0(0; m_W^2, m_{h_1}^2) - B_0(0; m_W^2, m_{h_3}^2) \right) \right. \right. \\ & \left. \left. - m_Z^2 \left(B_0(0; m_Z^2, m_{h_1}^2) - B_0(0; m_Z^2, m_{h_3}^2) \right) + B_{22}(0; m_W^2, m_{h_3}^2) - B_{22}(0; m_W^2, m_{h_1}^2) \right. \right. \\ & \left. \left. + B_{22}(0; m_Z^2, m_{h_1}^2) - B_{22}(0; m_Z^2, m_{h_3}^2) \right\} - \frac{1}{2} A_0(m_{H^\pm}^2) + B_{22}(0; m_{H^\pm}^2, m_{h_2}^2) \right. \\ & \left. + \cos^2 \theta_{23} \left(B_{22}(0; m_{H^\pm}^2, m_{A_0}^2) - B_{22}(0; m_{h_2}^2, m_{A_0}^2) \right) \right. \\ & \left. + \sin^2 \theta_{23} \left(B_{22}(0; m_{H^\pm}^2, m_{P_0}^2) - B_{22}(0; m_{h_2}^2, m_{P_0}^2) \right) \right. \\ & \left. + 4 \sin^4 \theta_W \left(m_\chi^2 B_0(0; m_\chi^2, m_\chi^2) - 2B_{22}(0; m_\chi^2, m_\chi^2) \right) \right] \end{aligned} \quad (3.13)$$

The deviation in the theoretical predictions for precision observables in SM (S_{SM} , T_{SM}) from the electroweak precision measurements in the experiments for $U \neq 0$ (S_{expt} , T_{expt}) are parameterised as [59]

$$\Delta S = S_{\text{expt.}} - S_{\text{SM}} = 0.01 \pm 0.10 \quad (3.14a)$$

$$\Delta T = T_{\text{expt.}} - T_{\text{SM}} = 0.03 \pm 0.12 \quad (3.14b)$$

Computing the precision observables numerically, we find that the allowed parameter space by the Higgs decays and LEP data satisfy the one sigma constraint for ΔS as given in equation (3.14a). In fact, the large uncertainty in the measurement allows the mass range between 50 - 1000 GeV for all scalars, pseudo-scalars and the VLL. However, the constrain on ΔT as given in equation (3.14b) further shrinks the allowed parameter region. We have depicted the one sigma density maps for the allowed region by the ΔT in the plane defined by the masses $m_{h_2} - m_{H^\pm}$, $m_{h_3} - m_{H^\pm}$, $m_{P_0} - m_{H^\pm}$ and $m_\chi - m_{H^\pm}$ in figure 5.

In the next section, we proceed with this constrained parameter space to look for viable explanation for the observed discrepancies in the measurements of the anomalous MDM for muon and electron.

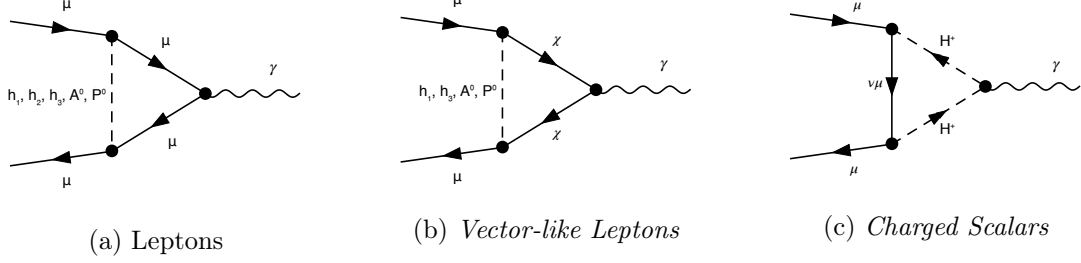


Figure 6: Dominant diagrams contributing to muon $g - 2$ at one-loop level.

4 Anomalous MDM of Leptons

We compute the additional model contribution (other than SM diagrams) to the Δa_l at one and two loops respectively.

In our model, the new one-loop contribution to Δa_l arises from the exchange of CP-even and odd scalars and from the charged Higgs and VLL diagrams. We draw the additional (other than those allowed by SM) dominant Feynman diagrams at one loop in figure 6 based on the Lagrangian given in equations (2.1d), (2.1f) and (2.1g).

The sum of the contributions to lepton Δa_l from the additional one-loop Feynman diagrams (other than SM) as shown in the figure 6 is calculated to be:

$$\delta a_l^{1\text{loop}} = \frac{1}{16\pi^2} \left[2 \frac{m_l^4}{v_{\text{SM}}^2} \left(\frac{\cos^2 \theta_{13}}{m_{h_1}^2} + \frac{\sin^2 \theta_{13}}{m_{h_3}^2} - \frac{1}{m_{h_{\text{SM}}}^2} \right) \mathcal{I}_1 + m_l^2 \left(\frac{\cos^2 \theta_{23}}{m_{A^0}^2} + \frac{\sin^2 \theta_{23}}{m_{P^0}^2} \right) y_1^2 \mathcal{I}_2 \right. \\ \left. + \frac{m_l^2}{m_{h_2}^2} y_1^2 \mathcal{I}_1 + \sum_{s_i=h_1, h_3, A^0, P^0} |y_{l\chi s_i}|^2 \frac{m_l^2}{m_{s_i}^2} \mathcal{I}_3 + |y_1|^2 \frac{m_l^2}{m_{H^\pm}^2} \mathcal{I}_4 \right] \quad (4.1a)$$

where the one loop functions \mathcal{I}_1 , \mathcal{I}_2 , \mathcal{I}_3 and \mathcal{I}_4 are defined in the appendix D in equations

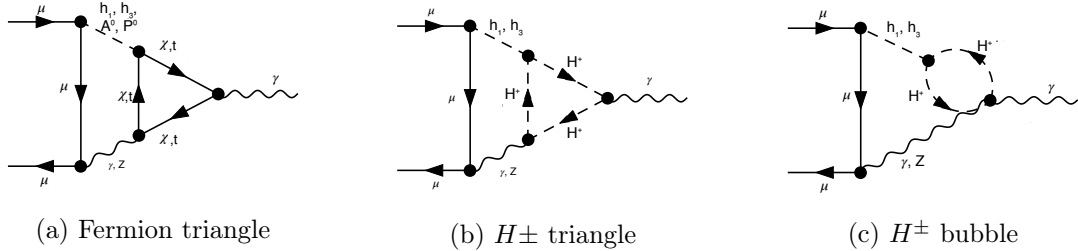


Figure 7: Dominant diagrams contributing to muon $g - 2$ at the two-loop level.

(D.1a), (D.1b), (D.1c) and (D.1d) respectively.

In order to obtain the common parameter-space satisfying both Δa_μ and Δa_e which are of opposite signs, it is imperative to analyse the nature of contribution by the mediating scalar/ pseudoscalar as given in figure 6. We observe that one-loop amplitudes in figure 6a are negative and positive corresponding to mediating pseudo-scalars and scalars respectively while loop amplitudes in figure 6b are positive for both pseudo-scalars and scalars except h_2 as it do not couples to VLL. The contribution from charged Higgs loop in figure 6c is negative and competitively much smaller in magnitude.

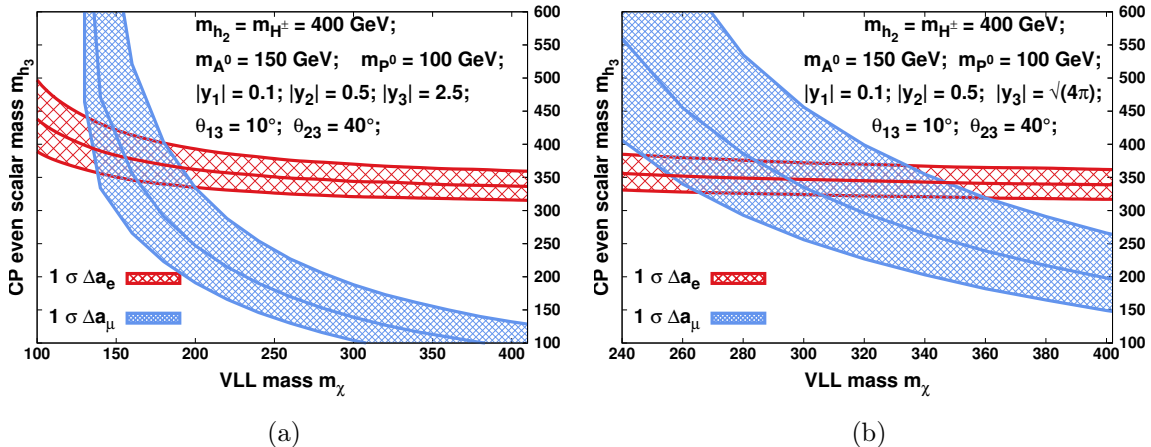


Figure 8: Colored solid contours and associated one sigma bands are shown in $m_{h_3} - m_\chi$ satisfying $\Delta a_\mu = (251 \pm 59) \times 10^{-11}$ [3] (in blue) and $\Delta a_e = [-88 \pm 28$ (expt.) ± 23 (α) ± 2 (theory)] $\times 10^{-14}$ [11] (in red). Contours are drawn for Yukawa couplings $|y_3| = 2.5$ and the perturbative limit $\sqrt{4\pi}$ in figures 8a and 8b respectively, while other physical masses, couplings and angles remain same for the both. The overlap of the two bands depict the common parameter space.

The contributions of two loop diagrams, some of which may dominate inspite of an additional loop suppression factor play a crucial role in the estimation of anomalous MDM. It is shown in the literature that the dominant two-loop Barr-Zee diagrams mediated by neutral scalars and pseudo-scalars can become relevant for certain mass scales so that their contribution to the muon anomalous MDM are of the same order to that of one loop diagrams [57].

In figure 7 we draw the dominant additional two-loop Barr-Zee diagrams (other than SM) contributing to the anomalous MDM of lepton which are based on the Lagrangian given in equations (2.1d), (2.1f) and (2.1g). The sum of the contributions to lepton Δa_l from the additional two-loop Feynman diagrams (other than SM) as shown in the figure 7 is calculated to be:

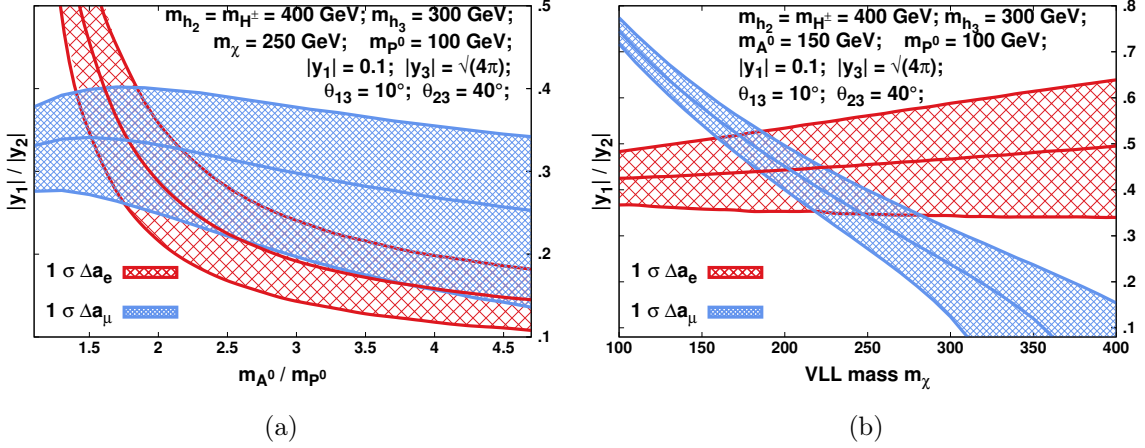


Figure 9: Colored solid contours and associated one sigma bands are shown in $|y_1|/|y_2| - m_{A^0}/m_{P^0}$ and $|y_1|/|y_2| - m_\chi$ planes satisfying $\Delta a_\mu = (251 \pm 59) \times 10^{-11}$ [3] (in blue) and $\Delta a_e = [-88 \pm 28 \text{ (expt.)} \pm 23 (\alpha) \pm 2 \text{ (theory)}] \times 10^{-14}$ [11] (in red). Contours are drawn with fixed $m_\chi = 250 \text{ GeV}$ and $m_{A^0} = 150 \text{ GeV}$ in figures 9a and 9b respectively while other physical masses, couplings and angles remain same for the both. The overlap of the two bands depict the common parameter space.

$$\begin{aligned}
\delta a_l^2 \text{ loop} = & \frac{\alpha_{em}}{4 \pi^3} \left[\frac{m_l}{v_{SM}} \frac{y_2}{\sqrt{2}} \sin \theta_{13} \cos \theta_{13} \left\{ f \left(\frac{m_\chi^2}{m_{h_3}^2} \right) - f \left(\frac{m_\chi^2}{m_{h_1}^2} \right) \right\} \right. \\
& + \frac{m_l}{v_{SM}} \frac{m_t}{v_{SM}} \left\{ \sin^2 \theta_{13} f \left(\frac{m_t^2}{m_{h_3}^2} \right) - \cos^2 \theta_{13} f \left(\frac{m_t^2}{m_{h_1}^2} \right) + f \left(\frac{m_t^2}{m_{h_{SM}}^2} \right) \right\} \\
& + \frac{y_1 y_2}{2} \frac{m_l}{m_\chi} \sin \theta_{23} \cos \theta_{23} \left\{ g \left(\frac{m_\chi^2}{m_{A^0}^2} \right) - g \left(\frac{m_\chi^2}{m_{P^0}^2} \right) \right\} \\
& \left. - \frac{m_l^2}{4} \frac{m_l}{v_{SM}^2} \left\{ \frac{\cos \theta_{13}}{m_{h_1}^2} g_{h_1 H^+ H^-} \tilde{f} \left(\frac{m_{H^\pm}^2}{m_{h_1}^2} \right) - \frac{\sin \theta_{13}}{m_{h_3}^2} g_{h_3 H^+ H^-} \tilde{f} \left(\frac{m_{H^\pm}^2}{m_{h_3}^2} \right) \right\} \right] \quad (4.2)
\end{aligned}$$

where the two loop functions f , g and \tilde{f} are defined in the appendix D in equations (D.2a), (D.2b) and (D.2c) respectively.

We find that the two loop amplitudes with VLL triangle in figure 7a are negative for mediating scalars and positive for mediating pseudo-scalars. The two-loop contributions of the charged Higgs in figure 7b and 7c are comparatively small and negative. The dominant Barr-Zee contributions are found to depend on the mixing angle θ_{23} , relative mass squared difference of the CP-odd scalars $m_{A^0}^2 - m_{P^0}^2$ and the Yukawa couplings y_1, y_2 .

The total contribution from one and two loop diagrams are computed for the constrained parameter space. Fixing the physical masses $m_{H^\pm} = m_{h_2} = 400 \text{ GeV}$, Yukawa coupling $|y_1| = 0.1$, $\Phi_1 - \Phi_3$ mixing angle θ_{13} at 10° and $\Phi_2 - \Phi_3$ mixing angle θ_{23} at

40° for our analysis, we vary m_{h_3} , m_χ , m_{A^0} , $|y_2|$ and $|y_3|$ to account for the contribution to anomalous MDM as observed in the experiments. Contours fulfilling the central value for Δa_μ [3] and Δa_e [11] quoted in equations (1.2) and (1.3) respectively are depicted in $m_\chi - m_{h_3}$ plane as shown in figure 8a for $|y_3| = 2.5$ and in figure 8b for the maximum allowed value of $|y_3| = \sqrt{4\pi}$ respectively. The overlapping region of the allowed one sigma bands for Δa_μ in blue and Δa_e in red exhibit the common parameter space satisfying both the experimental observations simultaneously. It is observed that overlapping region broadens for the large Yukawa coupling $|y_3|$ corresponding to a narrow mass range for m_{h_3} . In figure 9a and 9b we fix $m_{h_3} = 300$ GeV, $|y_3| = \sqrt{4\pi}$ and depict the one sigma band of contours in $|y_1|/|y_2| - m_{A^0}/m_{P^0}$ plane for $m_\chi = 250$ GeV and $|y_1|/|y_2| - m_\chi$ plane for $m_{A^0} = 150$ GeV respectively. We observe that a common parameter space for both are possible for $m_{A^0} \geq 1.5 m_{P^0}$ and $170 \text{ GeV} \lesssim m_\chi \lesssim 300 \text{ GeV}$. Choosing VLL mass at 250 GeV, $|y_3| = \sqrt{4\pi}$ and pseudo-scalar mass range such that $m_{A^0} > m_{P^0}$, we plot the narrow red one sigma band for Δa_e contours in $m_{h_3} - (m_{A^0}/m_{P^0})$ plane in figure 10 and observe that it completely overlaps with the broad blue one sigma band for Δa_μ contours. This constrains the m_{h_3} to be < 350 GeV.

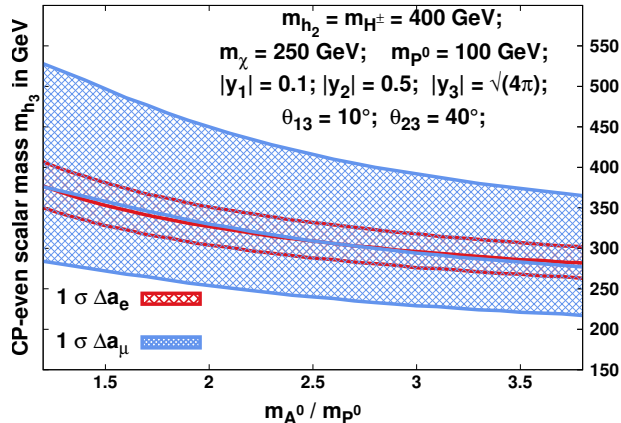


Figure 10: Colored solid contours and associated one sigma bands are shown in $m_{h_3} - m_{A^0}/m_{P^0}$ plane satisfying $\Delta a_\mu = (251 \pm 59) \times 10^{-11}$ [3] (in blue) and $\Delta a_e = [-88 \pm 28 \text{ (expt.)} \pm 23 \text{ (}\alpha\text{)} \pm 2 \text{ (theory)}] \times 10^{-14}$ [11] (in red). The overlap of the two bands depict the common parameter space.

5 Summary

In this article we considered an extended inert 2HDM model with an SM singlet complex scalar and a singlet vector like lepton field to explain the observed anomalies in the muon and electron dipole magnetic moments. The model parameters are expressed in terms of the physical masses and mixing angles of the CP even and odd scalars and are constrained from the Higgs decay to a pair of gauge Bosons at LHC, LEP data and electro-weak precision measurements. The contribution of scalars and vector-like lepton arises at the dominant one-loop and two-loop Barr-Zee diagrams. The CP even scalar one-loop contributions

to Δa_l are positive whereas the contribution from the CP-odd scalars is negative. The contribution of the VLL is important and decreases with the VLL mass. The Barr-Zee contributions mainly depend on the mixing angle θ_{23} and on relative mass squared difference of CP-odd scalars A^0 and P^0 and decreases with the VLL mass.

The constrained model is systematically analysed to accommodate both the experimental observations simultaneously. We depict the viable common parameter space through overlapping one sigma band of contours satisfying Δa_μ [3] and Δa_e [11] simultaneously in figures 8a, 8b, 9a, 9b and 10. We find that there exists a fairly large common parameter space where the anomalous magnetic moments of muon and electron can be explained.

Acknowledgments

We acknowledge the partial financial support from SERB grant CRG/2018/004889. HB acknowledges the CSIR JRF fellowship.

Appendix

A Scalar Couplings in terms of Mass Parameters

1. Since, LHC data favours a SM-like Higgs ~ 125 GeV, we align the mass of the lightest neutral Higgs state m_{h_1} coming predominantly from the doublet Φ_1 with the SM Higgs $m_{h_{SM}}$. In order to accommodate the 2σ uncertainty of the measured Higgs mass [59] the variation for $0.2 \leq \lambda_1 \leq 0.3$ may be allowed through mixing of $\Phi_1 - \Phi_3$.
2. The quartic parameter λ_2 appears only in the quartic interaction of Z_2 - odd particles and is therefore not constrained by our analysis.
3. Considering VEVs v_{SM} and v_s , mixing angles θ_{13} and θ_{23} , coupling λ_{13} and masses m_{22}^2 , $m_{h_1}^2$, $m_{h_2}^2$, $m_{h_3}^2$, $m_{H^\pm}^2$, $m_{A^0}^2$, and $m_{P^0}^2$ to be the free parameters, we can express m_{11}^2 , m_{33}^2 , λ_3 , λ_4 , λ_5 , λ_8 , λ_{11} and κ in terms of the above free parameters.
4. The Z_2 -odd charged scalar H^\pm comes solely from the second doublet, as in the IDM; its mass is given by

$$m_{H^\pm}^2 = \frac{1}{2} [-m_{22}^2 + v_{SM}^2 \lambda_3 + v_s^2 \lambda_{13}] \quad (\text{A.1})$$

λ_3 can be expressed in terms of free parameters λ_{13} , m_{22}^2 and the charged Higgs mass as

$$\lambda_3 = \frac{1}{v_{SM}^2} [2m_{H^\pm}^2 + m_{22}^2 - \lambda_{13} v_s^2] \quad (\text{A.2})$$

Notice, that the mass relations for the Z_2 -odd sector from the IDM hold, namely

$$m_{h_2}^2 = m_{H^\pm}^2 + \frac{v_{SM}^2}{2} [\lambda_4 + \lambda_5], \quad (\text{A.3})$$

$$m_{A^0}^2 + m_{P^0}^2 = m_{H^\pm}^2 + \frac{v_{SM}^2}{2} [\lambda_4 - \lambda_5] \quad (\text{A.4})$$

Therefore

$$\lambda_4 = \frac{1}{v_{\text{SM}}^2} [m_{h_2}^2 + m_{A^0}^2 + m_{P^0}^2 - 2 m_{H^\pm}^2] \quad (\text{A.5})$$

5. From pseudoscalars and heavy neutral scalar masses we have

$$\lambda_5 = \frac{1}{v_{\text{SM}}^2} [m_{h_2}^2 - m_{A^0}^2 - m_{P^0}^2] \quad (\text{A.6})$$

6. From mass relations for m_{h^0} and m_{S^0} given in equations (3.19) and (3.20) we get

$$\lambda_8 = \frac{1}{v_s^2} [m_{h_1}^2 + m_{h_3}^2 - \lambda_1 v_{\text{SM}}^2] \quad (\text{A.7})$$

$$\lambda_{11} = \frac{1}{v_{\text{SM}} v_s} (\lambda_1 v_{\text{SM}}^2 - \lambda_8 v_s^2) \tan(2\theta_{13}) \quad (\text{A.8})$$

7. The heavy neutral scalar mass from the Inert doublet is given as

$$m_{h_2}^2 = \frac{1}{2} [-m_{22}^2 + v_{\text{SM}}^2 \lambda_{345} + v_s^2 \lambda_{13}] \quad (\text{A.9})$$

Therefore

$$\lambda_{13} = \frac{1}{v_s^2} (2 m_{h_2}^2 + m_{22}^2 - v_{\text{SM}}^2 \lambda_{345}) \quad (\text{A.10})$$

B Definition of Loop Form Factors

The loop amplitudes are expressed in terms of dimensionless parameters τ and λ , which are essentially function of the masses of physical scalars/ pseudo-scalars and fermions.

$$\mathcal{M}_0^{\gamma\gamma}(\tau) = -\tau[1 - \tau f(\tau)] \quad (\text{B.1a})$$

$$\mathcal{M}_{1/2}^{\gamma\gamma}(\tau) = 2\tau[1 + (1 - \tau)f(\tau)], \quad (\text{B.1b})$$

$$\mathcal{M}_1^{\gamma\gamma}(\tau) = -[2 + 3\tau + 3\tau(2 - \tau)f(\tau)] \quad (\text{B.1c})$$

$$\mathcal{M}_0^{Z\gamma}(\tau, \lambda) = I_1^{Z\gamma}(\tau, \lambda) \quad (\text{B.1d})$$

$$\mathcal{M}_{1/2}^{Z\gamma}(\tau, \lambda) = [I_1^{Z\gamma}(\tau, \lambda) - I_2^{Z\gamma}(\tau, \lambda)] \quad (\text{B.1e})$$

$$\mathcal{M}_1^{Z\gamma}(\tau, \lambda) = c_W \left\{ 4 \left(3 - \frac{s_W^2}{c_W^2} \right) I_2^{Z\gamma}(\tau, \lambda) + \left[\left(1 + \frac{2}{\tau} \right) \frac{s_W^2}{c_W^2} - \left(5 + \frac{2}{\tau} \right) \right] I_1^{Z\gamma}(\tau, \lambda) \right\} \quad (\text{B.1f})$$

with

$$f(\tau) = \begin{cases} \arcsin^2\left(\frac{1}{\sqrt{\tau}}\right) & \text{for } \tau \geq 1, \\ -\frac{1}{4} \left[\log\left(\frac{1+\sqrt{1-\tau}}{1-\sqrt{1-\tau}}\right) - i\pi \right]^2 & \text{for } \tau < 1. \end{cases} \quad (\text{B.2})$$

The functions $I_1^{Z\gamma}$ and $I_2^{Z\gamma}$ are given by

$$\begin{aligned} I_1^{Z\gamma}(\tau, \lambda) &= \frac{\tau\lambda}{2(\tau-\lambda)} + \frac{\tau^2\lambda^2}{2(\tau-\lambda)^2} [f(\tau) - f(\lambda)] + \frac{\tau^2\lambda}{(\tau-\lambda)^2} \left[g\left(\frac{1}{\tau}\right) - g\left(\frac{1}{\lambda}\right) \right] \\ I_2^{Z\gamma}(\tau, \lambda) &= -\frac{\tau\lambda}{2(\tau-\lambda)} [f(\tau) - f(\lambda)] \end{aligned} \quad (\text{B.3})$$

Function $g(\tau)$ can be expressed as

$$g(\tau) = \begin{cases} \sqrt{\tau^{-1} - 1} \arcsin \sqrt{\tau} & \text{for } \tau \geq 1 \\ \frac{\sqrt{1 - \tau^{-1}}}{2} \left[\log \frac{1 + \sqrt{1 - \tau^{-1}}}{1 - \sqrt{1 - \tau^{-1}}} - i\pi \right] & \text{for } \tau < 1 \end{cases} \quad (\text{B.4})$$

C Veltman Passarino Loop Integrals

The A_0 , B_0 , B_{22} integrals are defined as

$$A_0(m^2) = m^2 (\Delta + 1 - \ln m^2), \quad (\text{C.1a})$$

$$B_0(q^2; m_1^2, m_2^2) = \Delta - \int_0^1 dx \ln(X - i\epsilon) \quad (\text{C.1b})$$

$$B_{22}(q^2; m_1^2, m_2^2) = \frac{1}{4}(\Delta + 1) \left[m_1^2 + m_2^2 - \frac{1}{3}q^2 \right] - \frac{1}{2} \int_0^1 dx X \ln(X - i\epsilon) \quad (\text{C.1c})$$

where $X \equiv m_1^2 x + m_2^2(1-x) - q^2 x(1-x)$ and $\Delta \equiv \frac{2}{4-d} + \ln(4\pi) + \gamma_E$ in d space-time dimensions.

D One loop and two loop functions for MDM

The one loop functions \mathcal{I}_1 , \mathcal{I}_2 , \mathcal{I}_3 and \mathcal{I}_4 required to compute one loop contribution to the MDM of leptons (4.1a) are defined as

$$\mathcal{I}_1(r^2) = \int_0^1 dx \frac{(1+x)(1-x)^2}{(1-x)^2 r^2 + x} \quad (\text{D.1a})$$

$$\mathcal{I}_2(r^2) = \int_0^1 dx \frac{-(1-x)^3}{(1-x)^2 r^2 + x}, \quad (\text{D.1b})$$

$$\mathcal{I}_3(r'^2) = \int_0^1 dx \frac{x(1-x)^2}{(1-x) r'^2 + x} \quad (\text{D.1c})$$

$$\mathcal{I}_4(r^2) = \int_0^1 dx \frac{-x(1-x)}{1 - (1-x) r^2} \quad (\text{D.1d})$$

with $r = \frac{m_l}{m_{s_i}}$, $r' = \frac{m_\chi}{m_{s_i}}$ and $s_i = h_1, h_2, h_3, A^0, P^0$.

The two-loop functions $f(r^2)$, $g(r^2)$ and $\tilde{f}(r^2)$ contributing to the MDM of leptons given in equation (4.2) are defined as

$$f(r^2) = \frac{r^2}{2} \int_0^1 dx \frac{1 - 2x(1-x)}{x(1-x) - r^2} \ln \left[\frac{x(1-x)}{r^2} \right] \quad (\text{D.2a})$$

$$g(r^2) = \frac{r^2}{2} \int_0^1 dx \frac{1}{x(1-x) - r^2} \ln \left[\frac{x(1-x)}{r^2} \right] \quad (\text{D.2b})$$

$$\tilde{f}(r^2) = \int_0^1 dx \frac{x(1-x)}{r^2 - x(1-x)} \ln \left[\frac{x(1-x)}{r^2} \right] \quad (\text{D.2c})$$

References

- [1] A. Keshavarzi, D. Nomura and T. Teubner, Phys. Rev. D **97** (2018) no.11, 114025 doi:10.1103/PhysRevD.97.114025 [arXiv:1802.02995 [hep-ph]].
- [2] T. Blum *et al.* [RBC and UKQCD], Phys. Rev. Lett. **121** (2018) no.2, 022003 doi:10.1103/PhysRevLett.121.022003 [arXiv:1801.07224 [hep-lat]].
- [3] B. Abi *et al.* [Muon g-2], Phys. Rev. Lett. **126** (2021) no.14, 141801 doi:10.1103/PhysRevLett.126.141801 [arXiv:2104.03281 [hep-ex]].
- [4] G. W. Bennett *et al.* [Muon g-2], Phys. Rev. D **73** (2006), 072003 doi:10.1103/PhysRevD.73.072003 [arXiv:hep-ex/0602035 [hep-ex]].
- [5] H. N. Brown *et al.* [Muon g-2], Phys. Rev. Lett. **86** (2001), 2227-2231 doi:10.1103/PhysRevLett.86.2227 [arXiv:hep-ex/0102017 [hep-ex]].
- [6] T. Aoyama, N. Asmussen, M. Benayoun, J. Bijnens, T. Blum, M. Bruno, I. Caprini, C. M. Carloni Calame, M. Cè and G. Colangelo, *et al.* Phys. Rept. **887** (2020), 1-166 doi:10.1016/j.physrep.2020.07.006 [arXiv:2006.04822 [hep-ph]].
- [7] S. Borsanyi, Z. Fodor, J. N. Guenther, C. Hoelbling, S. D. Katz, L. Lellouch, T. Lippert, K. Miura, L. Parato and K. K. Szabo, *et al.* Nature **593** (2021) no.7857, 51-55 doi:10.1038/s41586-021-03418-1 [arXiv:2002.12347 [hep-lat]].
- [8] A. Crivellin, M. Hoferichter, C. A. Manzari and M. Montull, Phys. Rev. Lett. **125** (2020) no.9, 091801 doi:10.1103/PhysRevLett.125.091801 [arXiv:2003.04886 [hep-ph]].
- [9] A. Keshavarzi, W. J. Marciano, M. Passera and A. Sirlin, Phys. Rev. D **102** (2020) no.3, 033002 doi:10.1103/PhysRevD.102.033002 [arXiv:2006.12666 [hep-ph]].
- [10] G. Colangelo, M. Hoferichter and P. Stoffer, Phys. Lett. B **814** (2021), 136073 doi:10.1016/j.physletb.2021.136073 [arXiv:2010.07943 [hep-ph]].
- [11] R. H. Parker, C. Yu, W. Zhong, B. Estey and H. Müller, Science **360** (2018), 191 doi:10.1126/science.aap7706 [arXiv:1812.04130 [physics.atom-ph]].
- [12] D. Hanneke, S. Fogwell and G. Gabrielse, Phys. Rev. Lett. **100** (2008), 120801 doi:10.1103/PhysRevLett.100.120801 [arXiv:0801.1134 [physics.atom-ph]].
- [13] G. F. Giudice, P. Paradisi and M. Passera, JHEP **11** (2012), 113 doi:10.1007/JHEP11(2012)113 [arXiv:1208.6583 [hep-ph]].
- [14] H. Davoudiasl and W. J. Marciano, Phys. Rev. D **98** (2018) no.7, 075011 doi:10.1103/PhysRevD.98.075011 [arXiv:1806.10252 [hep-ph]].

- [15] X. F. Han, T. Li, L. Wang and Y. Zhang, *Phys. Rev. D* **99** (2019) no.9, 095034 doi:10.1103/PhysRevD.99.095034 [arXiv:1812.02449 [hep-ph]].
- [16] M. Bauer, M. Neubert, S. Renner, M. Schnubel and A. Thamm, *Phys. Rev. Lett.* **124** (2020) no.21, 211803 doi:10.1103/PhysRevLett.124.211803 [arXiv:1908.00008 [hep-ph]].
- [17] G. Hiller, C. Hormigos-Feliu, D. F. Litim and T. Steudtner, *Phys. Rev. D* **102** (2020) no.7, 071901 doi:10.1103/PhysRevD.102.071901 [arXiv:1910.14062 [hep-ph]].
- [18] C. Cornella, P. Paradisi and O. Sumensari, *JHEP* **01** (2020), 158 doi:10.1007/JHEP01(2020)158 [arXiv:1911.06279 [hep-ph]].
- [19] I. Bigaran and R. R. Volkas, *Phys. Rev. D* **102** (2020) no.7, 075037 doi:10.1103/PhysRevD.102.075037 [arXiv:2002.12544 [hep-ph]].
- [20] S. Jana, V. P. K. and S. Saad, *Phys. Rev. D* **101** (2020) no.11, 115037 doi:10.1103/PhysRevD.101.115037 [arXiv:2003.03386 [hep-ph]].
- [21] L. Calibbi, M. L. López-Ibáñez, A. Melis and O. Vives, *JHEP* **06** (2020), 087 doi:10.1007/JHEP06(2020)087 [arXiv:2003.06633 [hep-ph]].
- [22] B. Dutta, S. Ghosh and T. Li, *Phys. Rev. D* **102** (2020) no.5, 055017 doi:10.1103/PhysRevD.102.055017 [arXiv:2006.01319 [hep-ph]].
- [23] K. F. Chen, C. W. Chiang and K. Yagyu, *JHEP* **09** (2020), 119 doi:10.1007/JHEP09(2020)119 [arXiv:2006.07929 [hep-ph]].
- [24] I. Doršner, S. Fajfer and S. Saad, *Phys. Rev. D* **102** (2020) no.7, 075007 doi:10.1103/PhysRevD.102.075007 [arXiv:2006.11624 [hep-ph]].
- [25] T. Han, S. K. Kang and J. Sayre, *JHEP* **02** (2016), 097 doi:10.1007/JHEP02(2016)097 [arXiv:1511.05162 [hep-ph]].
- [26] G. Aad *et al.* [ATLAS], [arXiv:2007.07830 [hep-ex]].
- [27] A. E. Cárcamo Hernández, Y. Hidalgo Velásquez, S. Kovalenko, H. N. Long, N. A. Pérez-Julve and V. V. Vien, [arXiv:2002.07347 [hep-ph]].
- [28] M. Badziak and K. Sakurai, *JHEP* **10** (2019), 024 doi:10.1007/JHEP10(2019)024 [arXiv:1908.03607 [hep-ph]].
- [29] M. Endo and W. Yin, *JHEP* **08** (2019), 122 doi:10.1007/JHEP08(2019)122 [arXiv:1906.08768 [hep-ph]].
- [30] F. J. Botella, F. Cornet-Gomez and M. Nebot, *Phys. Rev. D* **102** (2020) no.3, 035023 doi:10.1103/PhysRevD.102.035023 [arXiv:2006.01934 [hep-ph]].
- [31] E. Coluccio Leskow, G. D'Ambrosio, A. Crivellin and D. Müller, *Phys. Rev. D* **95** (2017) no.5, 055018 doi:10.1103/PhysRevD.95.055018 [arXiv:1612.06858 [hep-ph]].
- [32] A. Crivellin, D. Mueller and F. Saturnino, *Phys. Rev. Lett.* **127** (2021) no.2, 021801 doi:10.1103/PhysRevLett.127.021801 [arXiv:2008.02643 [hep-ph]].
- [33] E. J. Chun and J. Kim, *JHEP* **07** (2016), 110 doi:10.1007/JHEP07(2016)110 [arXiv:1605.06298 [hep-ph]].
- [34] A. Cherchiglia, D. Stöckinger and H. Stöckinger-Kim, *Phys. Rev. D* **98** (2018), 035001 doi:10.1103/PhysRevD.98.035001 [arXiv:1711.11567 [hep-ph]].
- [35] S. D. Thomas and J. D. Wells, *Phys. Rev. Lett.* **81** (1998), 34-37 doi:10.1103/PhysRevLett.81.34 [arXiv:hep-ph/9804359 [hep-ph]].

- [36] B. Barman, D. Borah, L. Mukherjee and S. Nandi, *Phys. Rev. D* **100** (2019) no.11, 115010 doi:10.1103/PhysRevD.100.115010 [arXiv:1808.06639 [hep-ph]].
- [37] R. Dermisek and A. Raval, *Phys. Rev. D* **88** (2013), 013017 doi:10.1103/PhysRevD.88.013017 [arXiv:1305.3522 [hep-ph]].
- [38] A. Falkowski, D. M. Straub and A. Vicente, *JHEP* **05** (2014), 092 doi:10.1007/JHEP05(2014)092 [arXiv:1312.5329 [hep-ph]].
- [39] A. Crivellin and M. Hoferichter, *JHEP* **07** (2021), 135 doi:10.1007/JHEP07(2021)135 [arXiv:2104.03202 [hep-ph]].
- [40] J. Liu, C. E. M. Wagner and X. P. Wang, *JHEP* **03** (2019), 008 doi:10.1007/JHEP03(2019)008 [arXiv:1810.11028 [hep-ph]].
- [41] M. Abdullah, B. Dutta, S. Ghosh and T. Li, *Phys. Rev. D* **100** (2019) no.11, 115006 doi:10.1103/PhysRevD.100.115006 [arXiv:1907.08109 [hep-ph]].
- [42] C. Arbeláez, R. Cepedello, R. M. Fonseca and M. Hirsch, *Phys. Rev. D* **102** (2020) no.7, 075005 doi:10.1103/PhysRevD.102.075005 [arXiv:2007.11007 [hep-ph]].
- [43] N. Haba, Y. Shimizu and T. Yamada, *PTEP* **2020** (2020) no.9, 093B05 doi:10.1093/ptep/ptaa098 [arXiv:2002.10230 [hep-ph]].
- [44] J. L. Yang, T. F. Feng and H. B. Zhang, *J. Phys. G* **47** (2020) no.5, 055004 doi:10.1088/1361-6471/ab7986 [arXiv:2003.09781 [hep-ph]].
- [45] C. Hati, J. Kriewald, J. Orloff and A. M. Teixeira, *JHEP* **07** (2020), 235 doi:10.1007/JHEP07(2020)235 [arXiv:2005.00028 [hep-ph]].
- [46] M. Trodden, *Rev. Mod. Phys.* **71** (1999), 1463-1500 doi:10.1103/RevModPhys.71.1463 [arXiv:hep-ph/9803479 [hep-ph]].
- [47] J. E. Kim, *Phys. Rept.* **150** (1987), 1-177 doi:10.1016/0370-1573(87)90017-2
- [48] J. M. Gerard and M. Herquet, *Phys. Rev. Lett.* **98** (2007), 251802 doi:10.1103/PhysRevLett.98.251802 [arXiv:hep-ph/0703051 [hep-ph]].
- [49] A. Broggio, E. J. Chun, M. Passera, K. M. Patel and S. K. Vempati, *JHEP* **11** (2014), 058 doi:10.1007/JHEP11(2014)058 [arXiv:1409.3199 [hep-ph]].
- [50] J. Cao, P. Wan, L. Wu and J. M. Yang, *Phys. Rev. D* **80** (2009), 071701 doi:10.1103/PhysRevD.80.071701 [arXiv:0909.5148 [hep-ph]].
- [51] V. Ilisie, *JHEP* **04** (2015), 077 doi:10.1007/JHEP04(2015)077 [arXiv:1502.04199 [hep-ph]].
- [52] T. Abe, R. Sato and K. Yagyu, *JHEP* **07** (2015), 064 doi:10.1007/JHEP07(2015)064 [arXiv:1504.07059 [hep-ph]].
- [53] L. Wang and X. F. Han, *JHEP* **05** (2015), 039 doi:10.1007/JHEP05(2015)039 [arXiv:1412.4874 [hep-ph]].
- [54] E. J. Chun, Z. Kang, M. Takeuchi and Y. L. S. Tsai, *JHEP* **11** (2015), 099 doi:10.1007/JHEP11(2015)099 [arXiv:1507.08067 [hep-ph]].
- [55] S. Dutta, A. Goyal and M. P. Singh, *JHEP* **07** (2019), 076 doi:10.1007/JHEP07(2019)076 [arXiv:1809.07877 [hep-ph]].
- [56] J. Kawamura, S. Okawa and Y. Omura, *JHEP* **08** (2020), 042 doi:10.1007/JHEP08(2020)042 [arXiv:2002.12534 [hep-ph]].

- [57] J. E. Chun and T. Mondal, JHEP **11** (2020), 077 doi:10.1007/JHEP11(2020)077 [arXiv:2009.08314 [hep-ph]].
- [58] Y. Amhis *et al.* [Heavy Flavor Averaging Group (HFAG)], [arXiv:1412.7515 [hep-ex]].
- [59] P.A. Zyla *et al.* (Particle Data Group), Prog. Theor. Exp. Phys. 2020, 083C01 (2020).
- [60] A. Denner, S. Heinemeyer, I. Puljak, D. Rebuszi and M. Spira, Eur. Phys. J. C **71** (2011), 1753 doi:10.1140/epjc/s10052-011-1753-8 [arXiv:1107.5909 [hep-ph]].
- [61] S. Heinemeyer *et al.* [LHC Higgs Cross Section Working Group], doi:10.5170/CERN-2013-004 [arXiv:1307.1347 [hep-ph]].
- [62] C. Bonilla, D. Sokolowska, N. Darvishi, J. L. Diaz-Cruz and M. Krawczyk, J. Phys. G **43** (2016) no.6, 065001 doi:10.1088/0954-3899/43/6/065001 [arXiv:1412.8730 [hep-ph]].
- [63] S. Schael *et al.* [ALEPH, DELPHI, L3, OPAL and LEP Electroweak], Phys. Rept. **532** (2013), 119-244 doi:10.1016/j.physrep.2013.07.004 [arXiv:1302.3415 [hep-ex]].
- [64] M. E. Peskin and T. Takeuchi, Phys. Rev. D **46** (1992), 381-409
- [65] W. J. Marciano and J. L. Rosner, Phys. Rev. Lett. **65** (1990), 2963-2966 [erratum: Phys. Rev. Lett. **68** (1992), 898]
- [66] D. C. Kennedy and P. Langacker, Phys. Rev. Lett. **65** (1990), 2967-2970 [erratum: Phys. Rev. Lett. **66** (1991), 395]
- [67] D. C. Kennedy, Phys. Lett. B **268** (1991), 86-88
- [68] J. R. Ellis, G. L. Fogli and E. Lisi, Phys. Lett. B **285** (1992), 238-244
- [69] H. E. Haber, [arXiv:hep-ph/9306207 [hep-ph]].